η' photoproduction on the nucleon in the quark model

Xian-Hui Zhong*
Department of Physics, Hunan Normal University, and Key Laboratory of Low-Dimensional Quantum Structures and Quantum Control of Ministry of Education, Changsha 410081, China

Qiang Zhao†
Institute of High Energy Physics, Chinese Academy of Sciences, Beijing 100049, China and
Theoretical Physics Center for Science Facilities, Chinese Academy of Sciences, Beijing 100049, China
(Received 17 October 2011; published 22 December 2011)

A chiral quark-model approach is adopted to study the $\gamma p \to \eta' p$ and $\gamma n \to \eta' n$. Good descriptions of the recent observations from CLAS and CBELSA/TAPS are obtained. Both of the processes are governed by $S_{11}(1535)$ and u channel background. Strong evidence of an $n = 3$ shell resonance $D_{15}(2080)$ is found in the reactions, which accounts for the bump-like structure around $W = 2.1$ GeV observed in the total cross section and excitation functions at very forward angles. The $S_{11}(1920)$ seems to be needed in the reactions, with which the total cross section near threshold for the $\gamma p \to \eta' p$ is improved slightly. The polarized beam asymmetries show some sensitivities to $D_{13}(1520)$, although its effects on the differential cross sections and total cross sections are negligible. There is no obvious evidence of the P-, D_{13}-, F-, and G-wave resonances with a mass around 2.0 GeV in the reactions.

DOI: 10.1103/PhysRevC.84.065204 PACS number(s): 13.60.Le, 14.20.Gk, 12.39.Jh, 12.39.Fe

I. INTRODUCTION

The threshold energy of the $\gamma p \to \eta' p$ and $\gamma n \to \eta' n$ reactions is above the second resonance region, which might be a good place to extract information of the less explored higher nucleon resonances around 2.0 GeV. Thus, the study of η' photoproduction becomes an interest topic in both experiment and theory. However, due to the small production rate for the η' via an electromagnetic probe, it had been a challenge for experiment to measure the η' production cross section in the photoproduction reaction [1–3].

Theoretical analyses can be found in the literature which were performed to interpret the old data of $\gamma p \to \eta' p$ [1–3]. Zhang *et al.* [4] first analyzed the old data with an effective Lagrangian approach, in which the off-shell contributions from the low-lying resonances in $1.5 \sim 1.7$ GeV were excluded. They considered that the main contribution to the photoproduction amplitude came from $D_{13}(2080)$. Li [5] and Zhao [6] also studied the reaction within a constituent quark-model approach. They found the dominance of S wave in the η' production, and the off-shell $S_{11}(1535)$ excitation played an important role near the η' threshold. They also predicted that effects of higher resonances in the $n = 3$ shell might be observable in experiment. The dominant role of $S_{11}(1535)$ was also suggested by Borasoy with the $U(3)$ baryon chiral perturbation theory [7], and Sibirtsev *et al.* with a hadronic model [8]. Considering the interferences between $S_{11}(1535)$ and the background (t-channel vector meson exchanges), they gave a reasonable description of the old data. In 2003 Chiang and Yang developed a Reggeized model for η and η' photoproduction on protons [9]. In this model, the differential cross-section data from Ref. [3] can be well described by the interference of an S_{11} resonance with a mass in the range of $1.932 \sim 1.959$ GeV and the t-channel Regge trajectory exchanges. In 2004 Nakayama and Haberzett [10] analyzed the differential cross-section data from Ref. [3] within a relativistic meson exchange model of hadronic interactions. They predicted that the observed angular distribution is due to the interference between the t channel and the nucleon resonances $S_{11}(1650)$ and $P_{11}(1880)$. Although there are some hints of higher nucleon resonances in the η' photoproduction process, it is not straightforward to extract them based on the old data with large uncertainties.

With the rapid development in experiment, recently, high-statistics and large-angle-coverage data for the $\gamma p \to \eta' p$ reaction have been reported by the CLAS Collaboration [11,12] and CBELSA/TAPS Collaboration [13], respectively. More recently, the measurements of the quasifree photoproduction of η' mesons off nucleons bound in the deuteron were also carried out by the CBELSA/TAPS Collaboration [14]. The recent new data not only provide us a good opportunity to better understand the reaction mechanism but also allows us to carry out a detailed investigation of the less explored higher nucleon resonances. Motivated by the new high-precision cross-section data obtained by the CLAS Collaboration [11], Nakayama and Haberzett [15] updated their fits and found that higher resonances with $J = 3/2$ might play important roles in reproducing the details of the measured angular distribution. A bump structure in the total cross around $W = 2.09$ GeV is predicted and might be caused by $D_{13}(2080)$ and/or $P_{13}(2100)$. In the quark model, Li [5] and Zhao [6] also found a bump structure around $W = 2.1$ GeV ($E_\gamma \simeq 2.0$ GeV) in the cross section by analyzing the old data. This structure comes from the $n = 3$ terms in the harmonic oscillator basis. The later higher-precision free-proton data from the CLAS Collaboration [11,12] indeed show a broad bump structure in the cross section around $W = 2.1$ GeV. This structure seems to also appear in the very recent quasifree-proton data and the data for inclusive quasifree $\gamma d \to (np)\eta'$ process [14].

*zhongxh@ihep.ac.cn
†zhaoq@ihep.ac.cn

To clarify the structures from the above analyses and observations, we present a systemic analysis of the recent experimental data for $\gamma p \to p\eta'$ and $\gamma n \to \eta' n$ in the framework of a chiral quark model as an improvement of the previous studies [5,6]. The chiral quark model has been well developed and widely applied to meson photoproduction reactions [16–27]. The details about the model can be found in Refs. [26,27]. Recently, we applied this model to study η photoproduction on the free and quasifree nucleons [28]. Good descriptions of the observations were obtained. In this work, we extend this approach to η' photoproduction. Given that η' and η are mixing states of flavor singlet and octet in the SU(3) flavor symmetry, we expect that some flavor symmetry relation can be applied to these two channels as a constraint on the model parameters. Moreover, since η' production has a higher threshold, the determination of the low-lying resonances in $1.5 \sim 1.7$ GeV in η photoproduction would be useful for estimating their off-shell contributions in η' photoproduction.

Similar to η production, an interesting difference between $\gamma p \to \eta' p$ and $\gamma n \to \eta' n$ is that in the γp reactions, contributions from states of representation $[70,^4 8]$ will be forbidden by the Moorhouse selection rule [29] in the SU(6)⊗O(3) symmetry. As a consequence, only states of $[56,^2 8]$ and $[70,^2 8]$ would contribute to $\gamma p \to \eta' p$. In contrast, all the octet states can contribute to the γn reactions. In another word, more states will be present in the γn reactions. Therefore, a combined study of the η' meson photoproduction on the proton and neutron should provide some opportunities for disentangling the role played by intermediate baryon resonances.

The paper is organized as follows. In Sec. II, a brief introduction of the chiral quark-model approach is given. The numerical results are presented and discussed in Sec. III. Finally, a summary is given in Sec. IV.

II. FRAMEWORK

In the chiral quark model, the s- and u-channel transition amplitudes for pseudoscalar-meson photoproduction on nucleons have been worked out in the harmonic oscillator basis in Ref. [26]. The t-channel contributions from vector meson exchange are not considered in this work. If complete sets of resonances are included in the s and u channels, the introduction of t-channel contributions might result in double counting [30,31].

It should be remarked that the amplitudes in terms of the harmonic oscillator principle quantum number n are the sum of a set of SU(6) multiplets with the same n. To see the contributions of individual resonances, we need to separate out the single-resonance-excitation amplitudes within each principle number n in the s channel. Taking into account the width effects of the resonances, the resonance transition amplitudes of the s channel can be generally expressed as [26]

$$\mathcal{M}_R^s = \frac{2M_R}{s - M_R^2 + iM_R\Gamma_R}\mathcal{O}_R e^{-(\mathbf{k}^2+\mathbf{q}^2)/6\alpha^2}, \tag{1}$$

where $\sqrt{s} = E_i + \omega_\gamma$ is the total energy of the system, α is the harmonic oscillator strength, M_R is the mass of the s-channel resonance with a width $\Gamma_R(\mathbf{q})$, and $\mathcal{O}_R$ is the separated operators for individual resonances in the s channel. In the Chew-Goldberger-Low-Nambu (CGLN) parametrization [32], the transition amplitude can be written with a standard form:

$$\begin{aligned}\mathcal{O}_R = {} & if_1^R \boldsymbol{\sigma}\cdot\boldsymbol{\epsilon} + f_2^R \frac{(\boldsymbol{\sigma}\cdot\mathbf{q})\boldsymbol{\sigma}\cdot(\mathbf{k}\times\boldsymbol{\epsilon})}{|\mathbf{q}||\mathbf{k}|} \\ & + if_3^R \frac{(\boldsymbol{\sigma}\cdot\mathbf{k})(\mathbf{q}\cdot\boldsymbol{\epsilon})}{|\mathbf{q}||\mathbf{k}|} + if_4^R \frac{(\boldsymbol{\sigma}\cdot\mathbf{q})(\mathbf{q}\cdot\boldsymbol{\epsilon})}{|\mathbf{q}|^2},\end{aligned} \tag{2}$$

where $\boldsymbol{\sigma}$ is the spin operator of the nucleon, $\boldsymbol{\epsilon}$ is the polarization vector of the photon, and $\mathbf{k}$ and $\mathbf{q}$ are incoming photon and outgoing meson momenta, respectively.

The $\mathcal{O}_R$ for the $n \leqslant 2$ shell resonances have been extracted in Ref. [26]. For the $n = 3$ shell, resonances are just around the η' production threshold, which might play important roles in the reaction. Thus, in this work we cannot treat them as degenerate any more. Their transition amplitudes $\mathcal{O}_R$ for S_{11}, D_{13}, D_{15}, G_{17}, and G_{19} waves are derived in the SU(6)⊗O(3) symmetric quark model limit, which have been given in Table I. The g factors that appear in Table I can be extracted from

TABLE I. CGLN amplitudes for s-channel resonances of the $n = 3$ shell in the SU(6)⊗O(3) symmetry limit. We have defined $A \equiv (\frac{\omega_m}{E_f+M_N}+1)|\mathbf{q}|$, $x \equiv \frac{|\mathbf{k}||\mathbf{q}|}{3\alpha^2}$, $P_l'(z) \equiv \frac{\partial P_l(z)}{\partial z}$, $P_l''(z) \equiv \frac{\partial^2 P_l(z)}{\partial z^2}$, $g_1 \equiv g_3^v - \frac{1}{8}g_2^v$, $g_2 \equiv g_3^v - \frac{1}{8}g_2^v$, and $g_3 \equiv g_3^s - \frac{1}{8}g_2^s$. ω_γ, ω_m, and E_f stand for the energies of the incoming photon, outgoing meson, and final nucleon, respectively, m_q is the constitute u or d quark mass, $1/\mu_q$ is a factor defined by $1/\mu_q = 2/m_q$, and $P_l(z)$ is the Legendre function with $z = \cos\theta$.

	f_1^R	f_2^R	f_3^R	f_4^R
S_{11}	$-\frac{i}{36}\frac{\omega_m\omega_\gamma}{\mu_q}(g_2+\frac{k}{2m_q}g_1)x^2$ $+\frac{i}{60}(g_1\frac{k}{m_q}+2g_2)Ax^3$	0	0	0
D_{13}	$\frac{i}{90}\frac{\omega_m\omega_\gamma}{\mu_q}(g_2+\frac{k}{2m_q}g_1)x^2$ $-\frac{i}{60}(g_1\frac{k}{m_q}+2g_2)Ax^3$	$\frac{i}{180}\frac{\omega_m\omega_\gamma^2}{\mu_q m_q}g_1x^2P_2'(z)-\frac{i}{105}$ $\frac{k}{m_q}(g_1+g_3/2)Ax^3P_2'(z)$	0	$-\frac{i}{90}\frac{\omega_m\omega_\gamma}{\mu_q m_q}g_2x^2P_2''(z)+\frac{i}{420}Ax^3$ $[14g_2-(g_1-g_3)\frac{k}{m_q}]P_2''(z)$
D_{15}	$\{-\frac{i}{90}\frac{\omega_m\omega_\gamma}{\mu_q}(g_2+\frac{k}{2m_q}g_1)x^2+\frac{i}{105}$ $[(g_1-\frac{1}{2}g_3)\frac{k}{m_q}+g_2]Ax^3\}P_3'(z)$	$-\frac{i}{180}\frac{\omega_m\omega_\gamma^2}{\mu_q m_q}g_1x^2P_2'(z)+\frac{i}{420}$ $\frac{k}{m_q}(5g_1-3g_3)Ax^3P_2'(z)$	$-\frac{i}{90}\frac{\omega_m\omega_\gamma}{\mu_q}g_2x^2P_3''(z)+\frac{i}{420}$ $[4g_2-(g_1-g_3)\frac{k}{m_q}]Ax^3P_3''(z)$	$\frac{i}{90}\frac{\omega_m\omega_\gamma}{\mu_q}g_2x^2P_2''(z)-\frac{i}{420}$ $[4g_2-(g_1-g_3)\frac{k}{m_q}]Ax^3P_2''(z)$
G_{17}	$\frac{-i}{1890}[(4g_1+5g_3)\frac{k}{m_q}$ $+18g_2]Ax^3P_3'(z)$	$\frac{-i}{210}(8g_2-g_1\frac{k}{m_q})Ax^3P_4'(z)$	$\frac{i}{1890}[(g_1-g_3)\frac{k}{m_q}-18g_2]Ax^3P_3''(z)$	$\frac{-i}{1890}[(g_1-g_3)\frac{k}{m_q}-18g_2]Ax^3P_4''(z)$
G_{19}	$i\frac{2k}{945m_q}(g_1-g_3)Ax^3P_5'(z)$	$i\frac{k}{378m_q}(g_1-g_3)Ax^3P_4'(z)$	$-i\frac{k}{1890m_q}(g_1-g_3)Ax^3P_5''(z)$	$i\frac{k}{1890m_q}(g_1-g_3)Ax^3P_4''(z)$

the quark model in the SU(6)⊗O(3) symmetry limit, and are defined by

$$g_3^v \equiv \langle N_f| \sum_j e_j I_j \sigma_{jz} |N_i\rangle, \tag{3}$$

$$g_3^s \equiv \langle N_f| \sum_j e_j I_j |N_i\rangle, \tag{4}$$

$$g_2^s \equiv \langle N_f| \sum_{i\neq j} e_j I_i \boldsymbol{\sigma}_i \cdot \boldsymbol{\sigma}_j |N_i\rangle/3, \tag{5}$$

$$g_2^v \equiv \langle N_f| \sum_{i\neq j} e_j I_i (\boldsymbol{\sigma}_i \times \boldsymbol{\sigma}_j)_z |N_i\rangle/2, \tag{6}$$

$$g_2^{v'} \equiv \langle N_f| \sum_{i\neq j} e_j I_i \sigma_{iz} |N_i\rangle, \tag{7}$$

where $|N_i\rangle$ and $|N_f\rangle$ stand for the initial and final states, respectively, and I_j is the isospin operator, which has been defined in Ref. [26]. For the η and η' production, the isospin operator is $I_j = 1$.

From Table I we can see that the $n = 3$ resonance amplitudes $f_i^R (i = 1, 2, 3, 4)$ for S and D waves contain two terms, which are in proportion to x^2 and x^3, respectively. The term $\mathcal{O}(x^3)$ is a higher-order term in the amplitudes for $x \equiv |\mathbf{k}||\mathbf{q}|/(3\alpha^2) \ll 1$. For the G_{17} and G_{19} waves, their amplitudes only contain the high-order term $\mathcal{O}(x^3)$, thus their contributions to the reactions should be small in the $n = 3$ shell resonances. Comparing the resonance amplitudes $f_i^R (i = 1, 2, 3, 4)$ for D_{13} with those for D_{15}, we find that

$$\left|f_1^R[D_{15}(n=3)]\right| > \left|f_1^R[D_{13}(n=3)]\right| P_3'(\cos\theta), \tag{8}$$

$$\left|f_i^R[D_{15}(n=3)]\right| > \left|f_i^R[D_{13}(n=3)]\right| \quad (i = 2, 3, 4), \tag{9}$$

for the η' and η photoproduction processes. The amplitude f_1^R for D_{13} is reaction angle independent, while the f_1^R for D_{15} depends on the reaction angle θ [i.e., $\propto P_3'(\cos\theta)$]. According to Eq. (8), at very forward and backward angles (i.e., $\cos\theta \simeq \pm 1$), we obtain

$$\left|f_1^R[D_{15}(n=3)]\right|_{\cos\theta\simeq\pm1} > 6\left|f_1^R[D_{13}(n=3)]\right|. \tag{10}$$

It shows that the magnitude of f_1^R at very forward and backward angles for D_{15} is about an order larger than that of D_{13}. Thus, the D_{15} partial wave is the main contributor to the η' and η photoproduction processes in the $n = 3$ shell resonances. At very forward and backward angle regions, the angle distributions might be sensitive to the D_{15} partial wave. We note that due to lack of experimental information and high density of states above 2 GeV, different representations that contribute to the same partial wave quantum number in the $n = 3$ shell are treated degenerately as one state, as listed in Table I.

Finally, the physical observables, differential cross section, and photon beam asymmetry are given by the following standard expressions [33]:

$$\frac{d\sigma}{d\Omega} = \frac{\alpha_e \alpha_{\eta'}(E_i + M_N)(E_f + M_N)}{16 s M_N^2} \frac{1}{2} \frac{|\mathbf{q}|}{|\mathbf{k}|} \sum_{i=1}^{4} |H_i|^2, \tag{11}$$

$$\Sigma = 2\mathrm{Re}(H_4^* H_1 - H_3^* H_2) \Big/ \sum_{i=1}^{4} |H_i|^2, \tag{12}$$

TABLE II. g factor in the amplitudes.

Reaction	g_3^v	g_3^s	g_2^s	g_2^v	$g_2^{v'}$	g_1	g_2	g_3
$\gamma p \to \eta'(\eta) p$	1	1	0	0	0	1	1	1
$\gamma n \to \eta'(\eta) n$	$-\frac{2}{3}$	0	$-\frac{2}{3}$	0	$-\frac{2}{3}$	$-\frac{2}{3}$	$-\frac{3}{4}$	$\frac{1}{12}$

where the helicity amplitudes H_i can be expressed by the CGLN amplitudes f_i [33,34].

III. CALCULATIONS AND ANALYSIS

A. Parameters

In our previous work, we studied η photoproduction off the quasifree neutron and proton from a deuteron target, where the masses, widths, and coupling strength parameters C_R of the $n \leqslant 2$ shell resonances had been determined [28]. In this work, the same parameter set is adopted. For the $n = 3$ shell resonances, S_{11}, D_{13}, D_{15}, G_{17}, and G_{19} waves, their transition amplitudes $\mathcal{O}_R$ have been derived in the SU(6)⊗O(3) symmetric quark-model limit, which are given in Table I. The various g factors in these amplitudes for η' photoproduction on the nucleons have been derived in the SU(6)⊗O(3) symmetry limit, which are listed in Table II. Their resonance parameters are determined by the experimental data. The determined mass and width for D_{15} are $M \simeq 2080$ MeV and $\Gamma \simeq 80$ MeV, respectively, while the determined mass and width of S_{11} are $M \simeq 1920$ MeV and $\Gamma \simeq 90$ MeV. It should be pointed out that the reactions are insensitive to the masses and widths of G- and D_{13}-wave states in the $n = 3$ shell. Thus, in the calculation we roughly take their mass and width with $M = 2100$ MeV and $\Gamma = 150$ GeV, respectively.

There are two overall parameters, the constituent quark mass m_q and the harmonic oscillator strength α, from the transition amplitudes. In the calculations we adopt the standard values in the the quark model, $m_q = 330$ MeV and $\alpha^2 = 0.16$ GeV^2.

To take into account the relativistic effects, the commonly applied Lorentz boost factor is introduced in the resonance amplitude for the spatial integrals [18], which is

$$\mathcal{O}_R(\mathbf{k}, \mathbf{q}) \to \gamma_k \gamma_q \mathcal{O}_R(\gamma_k \mathbf{k}, \gamma_q \mathbf{q}), \tag{13}$$

where $\gamma_k = M_N/E_i$ and $\gamma_q = M_N/E_f$.

The $\eta' NN$ coupling is a free parameter in the present calculations and to be determined by the experimental data. In the present work the overall parameter $\eta' NN$ coupling $\alpha_{\eta'}$ is set to be the same for both $\gamma n \to \eta' n$ and $\gamma p \to \eta' p$. The fitted value $g_{\eta' NN} \simeq 1.86$ (i.e., $\alpha_{\eta'} \equiv g_{\eta' NN}^2/4\pi = 0.275$) is in agreement with that in Ref. [15], where the upper limit of $g_{\eta' NN}$ was suggested to be $g_{\eta' NN} \lesssim 2$. In our previous work, we determined the ηNN coupling, i.e., $g_{\eta NN} \simeq 2.13$ [28]. This allows us to examine the η-η' mixing relation for their nonstrange components production,

$$\tan\phi_P = \frac{g_{\eta' NN}}{g_{\eta NN}}, \tag{14}$$

which gives $\phi_P \simeq 41.2^\circ$. This value is within the range of $\phi_P = \theta_P + \arctan\sqrt{2} \simeq 34^\circ \sim 44^\circ$, where $\theta_P \simeq -20^\circ \sim -10^\circ$ is

the flavor singlet and octet mixing angle. The favored value for ϕ_P implies a flavor symmetry between η and η' production.

Since the single resonance excitation amplitudes can be separated out for $n \leqslant 2$ shells, the $\eta' N^* N$ coupling form factor in principle can be extracted by taking off the electromagnetic (EM) helicity amplitudes. The expressions are similar to those extracted in η meson photoproduction [28] apart from the overall $g_{\eta' NN}$ coupling constant. For higher excited states in $n = 3$, due to the lack of information about their EM excitation amplitudes and high density of states above the 2 GeV mass region, we treat all SU(6) multiplets that contribute to the same quantum number in $n = 3$ to be degenerate. In this sense, the partial waves in Table I are collective amplitudes from both **56** and **70** representations.

B. $\gamma p \to \eta' p$

The chiral quark-model studies of $\gamma p \to \eta' p$ have been carried out in Refs. [5,6], where a bump structure around $E_\gamma = 2$ GeV is found arising from the $n = 3$ terms in the harmonic oscillator basis. However, which partial wave contributes to this structure cannot be studied in detail since only a few data points were available at that time. The improvement of the experimental situations not only gives us a good opportunity to better understand the $\gamma p \to \eta' p$ process, but also allows us to carry out a detailed investigation of the resonances in the higher mass region.

In Fig. 1, we have plotted the differential cross sections. It shows that our calculations are in good agreement with the data from threshold up to $E_\gamma \simeq 2.4$ GeV. $S_{11}(1535)$ plays a dominant role in the reaction; switching off its contributions, the differential cross sections are underestimated drastically. The important role of $S_{11}(1535)$ in the $\gamma p \to \eta' p$ is also predicted in the previous chiral quark-model study [5,6] and the hadronic model study with the exchange of vector mesons [8,15]. It should be mentioned that the $S_{11}(1535)$ is treated as a mixed state by the mixing of $[70,^2 8]$ and $[70,^4 8]$ [28], where the mixing angle is in agreement with the recent study [35].

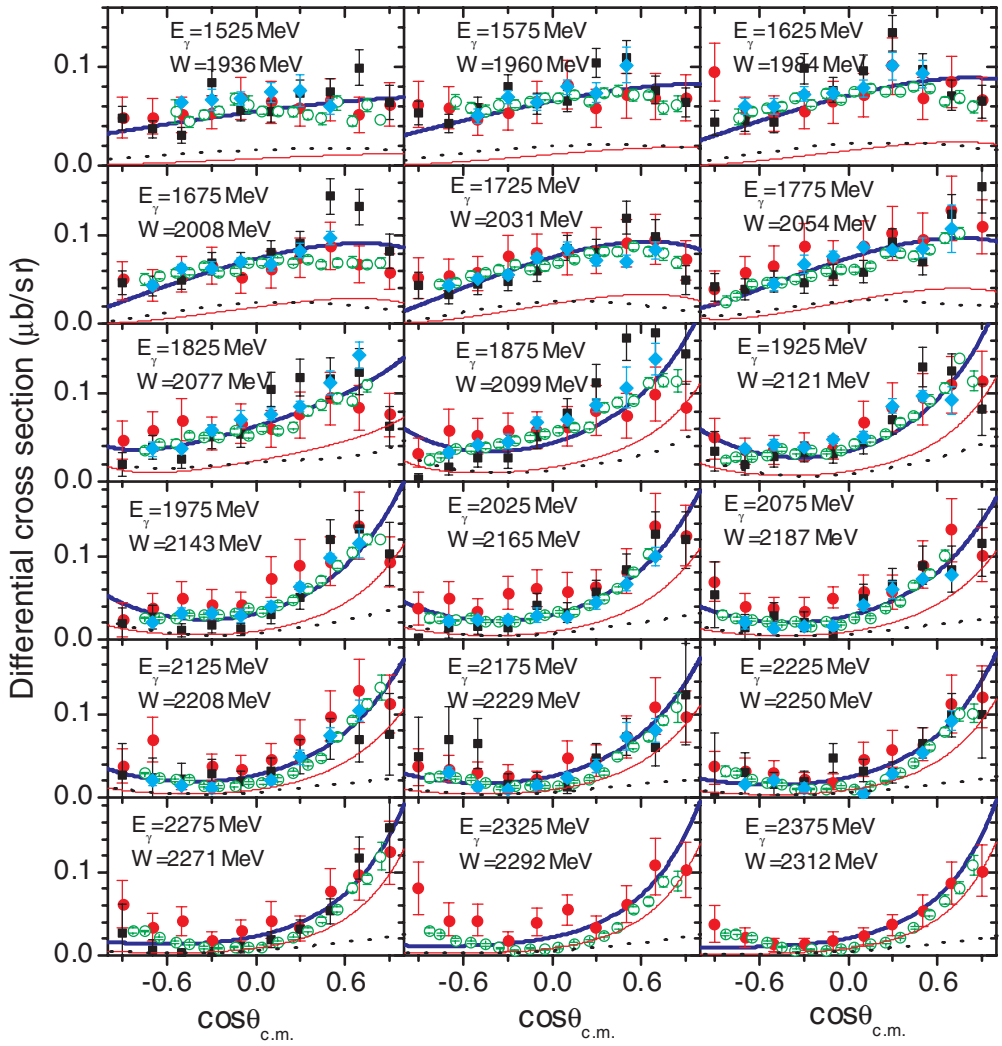

FIG. 1. (Color online) Differential cross sections for the η' photoproduction off the free proton at various beam energies. The data are taken from Refs. [13] (solid circles), [12] (open circles), and [11] (diamonds). The quasifree data from Ref. [14] (squares) are also included. The bold solid curves stand for the full model calculations. The thin solid and dotted curves stand for the results without $S_{11}(1535)$ and background u-channel contributions, respectively.

Furthermore, the u channel plays an important role in the reactions as well. The dotted curves in Fig. 1 show that without the contributions of the u channel, the cross sections will be underestimated significantly. It should be pointed out that the forward peaks in the differential cross sections are mainly caused by the u-channel backgrounds. The crucial role of nonresonant background contributions in the $\gamma p \to \eta' p$ is also predicted in Refs. [8,15], where the t-channel vector meson exchanges are the main nonresonant contributions. In this work, the t-channel contributions are not considered. Since a complete set of resonances in the s and u channels is included and the η' threshold is rather high, we do not include the t-channel exchanges to avoid the double counting problem [19,30,31].

It is interesting to see that $D_{15}(2080)$ in the $n = 3$ shell plays a crucial role in the reaction. It causes a shape change in the differential cross section around the $D_{15}(2080)$ mass region (i.e., $E_\gamma \simeq 1.8$ GeV). In Fig. 2 we demonstrate the interfering effects of $D_{15}(2080)$ by switching it off in the differential cross section below and above the mass of $D_{15}(2080)$. It could be obvious evidence of $D_{15}(2080)$ in the $\gamma p \to \eta' p$ process. We have noted that another D-wave state, $D_{13}(2080)$, was predicted to have significant effects on the reaction in Refs. [4,15]. However, in our approach the contributions of the D-wave states with $J^P = 3/2^-$ in the $n = 3$ shell are negligible. The dominant features of D_{15} in the D-wave states can be well understood from their amplitudes, which has been discussed in Sec. II. The amplitude f_1^R for D_{15} is in proportion to $P_3'(\cos\theta) = (15\cos^2\theta - 3)/2$, which can naturally explain the strong effects of $D_{15}(2080)$ on the deferential cross sections at forward and backward angles (i.e., $\cos\theta \simeq \pm 1$).

The effects of $D_{15}(2080)$ can be expected in $\gamma p \to \eta p$ taking into account the mixing between η' and η. A recent quark-model study of η photoproduction in the high-energy region has reported effects from $D_{15}(2080)$ [22,23]. Evidence of $D_{15}(2080)$ was also found by a partial wave analysis of

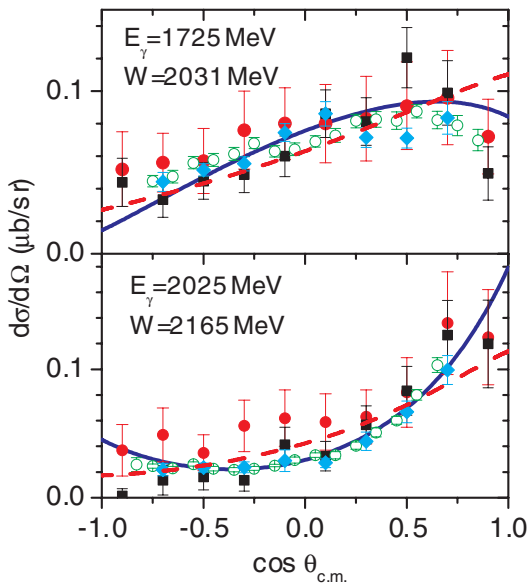

FIG. 2. (Color online) Same as Fig. 1. The dashed curves stand for the results without $D_{15}(2080)$.

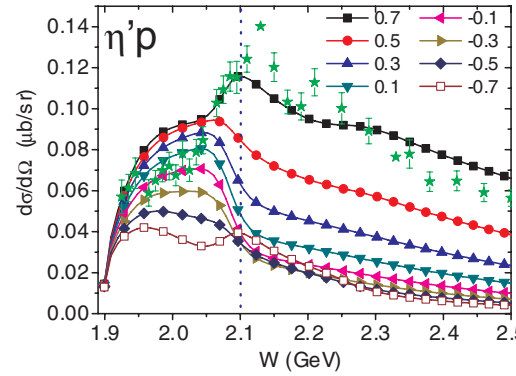

FIG. 3. (Color online) Fixed-angle excitation functions for $\gamma p \to \eta' p$ as a function of center-of-mass energy W for eight $\cos\theta$, which have been labeled on the plot. The stars stand for the data from Ref. [12] for $\cos\theta = 0.7$.

the η photoproduction data from CB-ELSA [36] in the Bonn-Gatchina (BnGa) model [37]. Its contribution to $\gamma p \to K^+\Lambda$ was also reported [38]. Our analysis of the partial wave amplitudes in Sec. II also suggests that the D_{15} amplitude plays a dominant role in the $n = 3$ shell D-wave states in K photoproduction.

We also mention that $P_{13}(1900)$ can slightly enhances the differential cross sections around the η' production threshold as found in the previous studies as well [6,9]. It has a similar behavior to the u channel, although its contribution is much less than that of the u channel. It could be difficult to identify

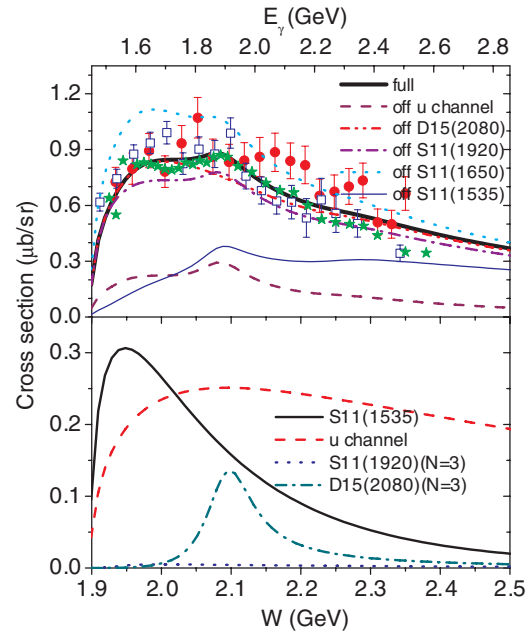

FIG. 4. (Color online) Cross sections for η' photoproduction off the free proton. The data are taken from Refs. [13] (solid circles) and [12] (stars). The quasifree data from Ref. [14] (squares) are also included. In the upper panel, the curves show the full model result and the results obtained by switching off the contributions from $S_{11}(1535)$, $S_{11}(1650)$, $S_{11}(1920)$, $D_{15}(2080)$, and u channel (see legend). In the lower panel, the partial cross sections for the main contributors are indicated explicitly by different curves.

$P_{13}(1900)$ in the $\gamma p \to \eta' p$ process in the cross-section measurement. Similar conclusion is found in Ref. [9]. In our study, contributions from other individual resonances are rather small, and we do not find obvious signals for states, such as higher S_{11} states.

In Fig. 3 we have plotted the fixed-angle excitation functions for $\gamma p \to \eta' p$. Our calculations show that at very forward (e.g., $\cos\theta = 0.7$) and backward scattering angles (e.g., $\cos\theta = -0.7$), there is a bump around $W = 2.1$ GeV. At forward angles, a similar structure appears clearly in the recent data from the CLAS Collaboration [12] (see the stars in Fig. 3). In our approach the bump structure is caused by $D_{15}(2080)$. At backward angles, due to the small η' production cross section, it might be difficult to observe such an enhancement in the excitation functions around $W = 2.1$ GeV.

Finally, the total cross section and exclusive cross sections for several single resonances are illustrated in Fig. 4. The data can be reasonably well described. The recent data show a small bump-like structure around $W = 2.1$ GeV (see the stars) [12], which in our approach is due to the interferences of $D_{15}(2080)$ with other partial waves. Switching off the contribution of $D_{15}(2080)$, we find that the bump-like structure disappears (see the dash-dot-dotted curve in the upper panel of Fig. 4). It should be mentioned that the bump-like structure around $W = 2.1$ GeV was explained by the effects of $D_{13}(2080)$ and/or $P_{11}2100$ in Ref. [15].

In Fig. 4, the dominant role of $S_{11}(1535)$ and the u-channel background can be obviously seen from their exclusive cross sections, which are much larger than that of other resonances. The large cross section around the η' production threshold mainly comes from the interferences of $S_{11}(1535)$ and the u channel. Switching off either of them, we find that the cross section will be underestimated drastically. The calculation shows that both $S_{11}(1650)$ and $S_{11}(1920)$ have rather small effects on the cross section around the η' production threshold (see the dotted and dash-dotted curves in the upper panel of Fig. 4). It should be noted that, although $S_{11}(1920)$ has a small contribution to the cross section, its mass favors to be less than 1950 MeV. Otherwise, we cannot reproduce the present cross sections in the region of $W < 2.0$ GeV. The mass of $S_{11}(1920)$

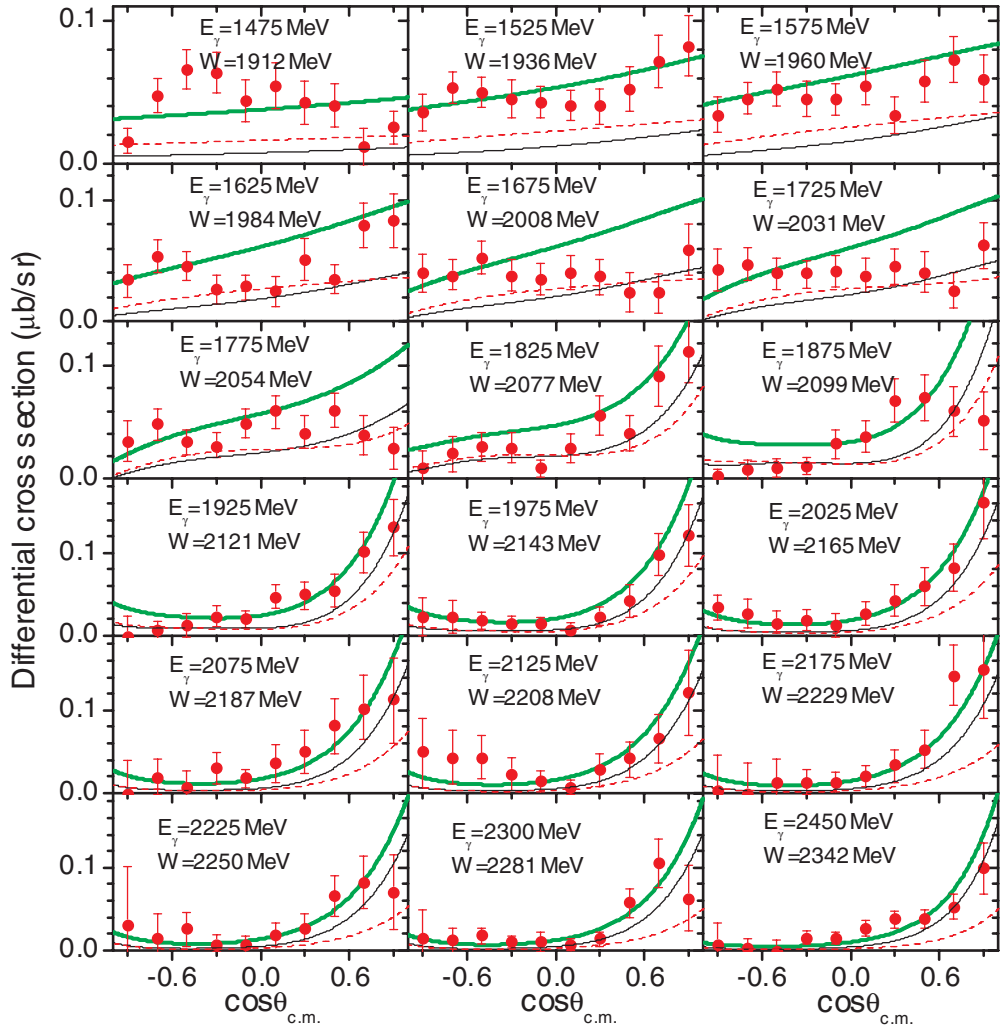

FIG. 5. (Color online) Differential cross sections for $\gamma n \to \eta' n$ at various beam energies. The data are taken from Ref. [14] (squares). The bold solid curves stand for the full model calculations. The thin solid and dotted curves stand for the results without $S_{11}(1535)$ and background u-channel contributions, respectively.

extracted here is close to that obtained in Ref. [9]. $S_{11}(1920)$ might correspond to the $S_{11}(2090)$ listed by the Particle Data Group as a one-star resonance with a mass varying from 1880 to 2180 MeV [39].

In brief, the $\gamma p \to \eta' p$ reaction is dominated by $S_{11}(1535)$ and u-channel contributions. The constructive interference between them accounts for the large cross section near threshold. $D_{15}(2080)$ plays an important role in the reaction. It has obvious effects on the angle distributions, and is responsible for the bump-like structure around $W = 2.1$ GeV observed in the cross section. Weak signal of $S_{11}(1920)$ might be extracted from the cross section near threshold. The reaction is less sensitive to the other intermediate states.

C. $\gamma n \to \eta' n$

Recently, the CBELSA/TAPS Collaboration observed the $\gamma n \to \eta' n$ process for the first time [14]. The data had been compared to fits with the Nakayama and Haberzettl (NH) [15] and MAID [9] models. There exists large disagreement between model fits and the experimental observations. As mentioned earlier, in $\gamma n \to \eta' n$ states of $[70,^4 8]$ representation can contribute here, while they are forbidden in $\gamma p \to \eta' p$ by the Moorhouse selection rule [29]. Therefore, we expect that more information about the s-channel resonances can be gained in the study of $\gamma n \to \eta' n$. For instance, as the only D_{15} state in the first orbital excitations and belonging to $[70,^4 8]$, $D_{15}(1675)$ can only be excited by γn instead of γp. We also note that in this work the nuclear Fermi motion effects have been neglected since they are negligible according to a recent analysis [14].

In Fig. 5, the differential cross sections at various beam energies have been plotted. It shows that our quark model fits are in good agreement with the recent CBELSA/TAPS measurements in the beam energy region $E_\gamma > 1.9$ GeV [14]. However, in the region $E_\gamma < 1.9$ GeV, we cannot reproduce the data well, especially at the forward angles. In this region, our results are close to the fits of the NH model [15].

Similar to $\gamma p \to \eta' p$, the differential cross sections for $\gamma n \to \eta' n$ are governed by the $S_{11}(1535)$ and u-channel contributions. Switching off either of them (see thin solid and dashed curves), we find that the cross sections would be underestimated significantly. It shows that $S_{11}(1535)$ dominates near threshold ($E_\gamma < 1.9$ GeV), and strongly enhances the cross section. At higher energies ($E_\gamma > 2.0$ GeV), the u channel becomes the main contributor in the differential cross sections. The role of $D_{15}(2080)$ in the $\eta' n$ channel is similar to that in the $\eta' p$ channel. It slightly enhances the cross sections at forward angles in the higher energy region ($E_\gamma > 1.9$ GeV). However, the present data for $\gamma n \to \eta' n$ seems not precise enough to confirm $D_{15}(2080)$ in the reaction. Again, we find that the contribution from $P_{13}(1900)$ is negligibly small and might be difficult to identify in the cross-section measurement.

In Fig. 6, the total cross section and the exclusive cross sections of several single resonances are shown. Again, we see the dominance of $S_{11}(1535)$ and u channel in the cross sections.

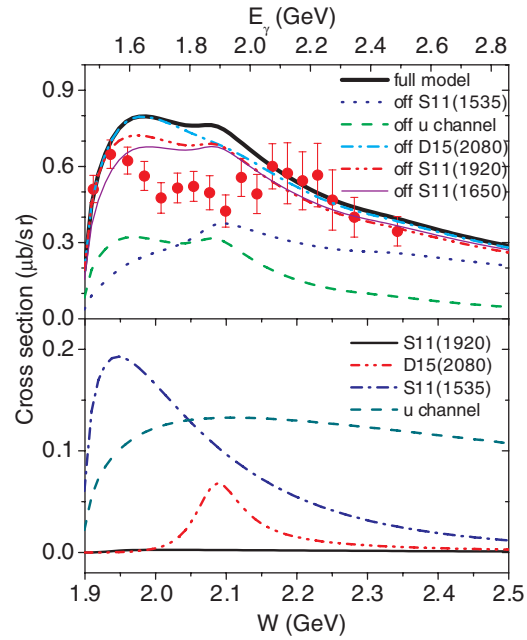

FIG. 6. (Color online) Cross sections for the $\gamma n \to \eta' n$ process. The data are taken from Ref. [14]. In the upper panel, the curves correspond to the full model result and the results obtained by switching off the contributions from $S_{11}(1535)$, $S_{11}(1650)$, $S_{11}(1920)$, $D_{15}(2080)$, and u channel (see legend). In the lower panel, the partial cross sections for the main contributors are indicated explicitly by different curves.

Some interfering effects between $S_{11}(1650)/S_{11}(1920)$ and $S_{11}(1535)$ can be seen near threshold. There also exist some discrepancies in the low energy region, i.e., $E_\gamma \simeq 1.6 \sim 2.0$ GeV, between our model results and experimental data. Our model suggests two bump structures in the total cross section. The first one around $W = 1.95$ GeV is mainly caused by $S_{11}(1535)$, while the second around $W = 2.1$ GeV is caused by $D_{15}(2080)$. The data [14] seem to show a bump structure around $W = 1.95$ GeV, while the second bump structure around $W = 2.1$ GeV cannot be identified due to the large experimental uncertainties.

In Ref. [14], the data for the inclusive quasifree $\gamma d \to np\eta'$ cross section, σ_{np}, are also presented. It shows that the σ_{np} is nearly equal to the sum of the free-proton (σ_p) and free-neutron (σ_n) cross sections. Interestingly, the data indicate two broad bump structures in the cross section around $W = 1.95$ and $W = 2.1$ GeV. To compare with the data, we plot our calculations of $(\sigma_p + \sigma_n)$ in Fig. 7, which appears to be compatible with the data, although the cross section around $W = 2.05$ GeV is slightly overestimated. In our approach, the second bump structure in the inclusive quasifree $\gamma d \to np\eta'$ cross section is caused by $D_{15}(2080)$. This contribution seems to be highlighted in $\gamma d \to np\eta'$ as a summed-up effect from both proton and neutron reactions. Further improved measurement should be able to clarify the underlying mechanisms that produce the bump structures.

In Fig. 8 the excitation functions for $\gamma n \to \eta' n$ as a function of the center-of-mass energy W at various angles are plotted. It is sensitive to the presence of $D_{15}(2080)$ as shown

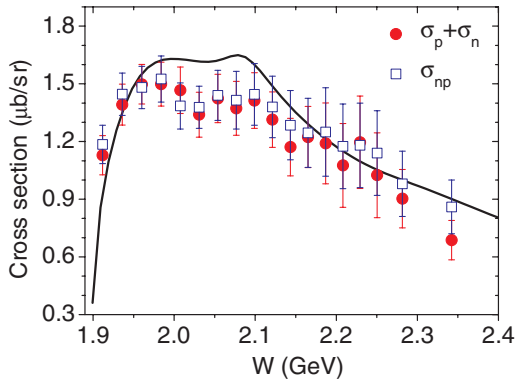

FIG. 7. (Color online) Data for inclusive quasifree $\gamma d \to np\eta'$ cross section (σ_{np}) and the sum of quasifree-proton and quasifree-neutron cross sections ($\sigma_p + \sigma_n$). The solid curve corresponds to our results of the sum of free-proton and free-neutron cross sections.

by the drastic enhancement at very forward angles around $W = 2.1$ GeV. This feature is similar to that in $\gamma p \to \eta' p$ (see Figs. 3 and 8).

Polarization observables should be more sensitive to the underlying mechanisms. In Fig. 9, we plot the polarized beam asymmetries for $\gamma p \to \eta' p$ (left) and $\gamma n \to \eta' n$ (right). The beam asymmetries for both of the precesses are sensitive to $S_{11}(1535)$, $D_{13}(1520)$, $D_{15}(2080)$, and u-channel contributions (see the bottom of Fig. 9). A sudden change of the beam asymmetries around $E_\gamma \simeq 1.8$ GeV [i.e., the threshold of $D_{15}(2080)$] can be seen, which is mainly caused by the $D_{15}(2080)$. Furthermore, it shows that the beam asymmetry for $\gamma n \to \eta' n$ (Σ_n) is quite similar to that of $\gamma p \to \eta' p$ (Σ_p) up to $E_\gamma \simeq 1.8$ GeV. In this energy region the beam asymmetry is nearly symmetric in the forward and backward directions. Above $E_\gamma \simeq 1.9$ GeV, obvious differences show up between Σ_n and Σ_p. It should be noted that the contribution of $D_{13}(1520)$ does not appear to be significant in the hadronic model studies. Therefore, experimental measurement of the polarized beam asymmetries should provide a test for various models.

In brief, $\gamma n \to \eta' n$ has features similar to those of $\gamma p \to \eta' p$. Both reactions are dominated by $S_{11}(1535)$ and u-channel contributions. We predict that $D_{15}(2080)$ should

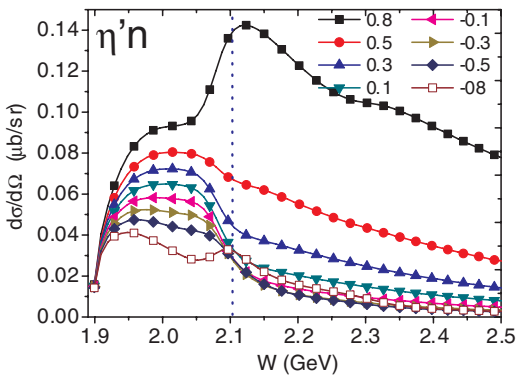

FIG. 8. (Color online) Fixed-angle excitation functions for $\gamma n \to \eta' n$ as a function of center-of-mass energy W for eight values of $\cos\theta$.

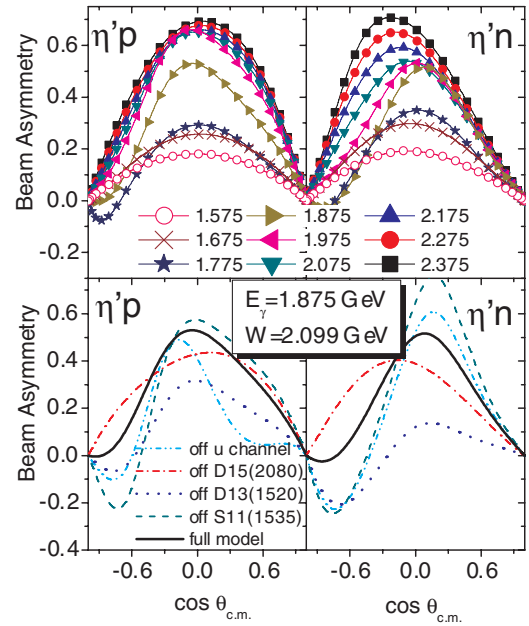

FIG. 9. (Color online) Predicted beam asymmetries at nine beam energies ($E_\gamma = 1.575 \sim 2.375$ GeV) for $\gamma p \to \eta' p$ and $\gamma n \to \eta' n$.

have significant contributions to $\gamma n \to \eta' n$, and the polarized beam asymmetries might be sensitive to its presence in the transition amplitude. Finally, we should point out that although $D_{15}(1675)$ has a significant contribution to the $\gamma n \to \eta n$ process, its contribution to $\gamma n \to \eta' n$ is negligible.

IV. SUMMARY

In this work, we have studied the η' photoproduction off the proton and neutron within a chiral quark model. A good description of the recent experimental data for both processes is achieved. Due to the similar reaction mechanism for both processes, it is understandable that some similar features exist in both reactions as manifested in the cross sections, excitation functions, and polarized beam asymmetries.

The large peak of the cross section around threshold for both processes mainly accounts for the constructive interferences between $S_{11}(1535)$ and the u-channel background. Strong evidence of $D_{15}(2080)$ has been found in the reactions, with which we can explain the following recent high-statistics observations for the $\gamma p \to \eta' p$ reaction from CLAS Collaboration: (i) the sudden change of the shape of the differential cross section around $E_\gamma = 1.8$ GeV, (ii) the bump-like structure in the total cross section around $W = 2.1$ GeV ($E_\gamma \simeq 1.9$ GeV), and (iii) the peak around $W = 2.1$ GeV in the excitation functions at very forward angles. Furthermore, $D_{15}(2080)$ also accounts for the bump-like structure at $W \simeq 2.1$ GeV in the inclusive quasifree $\gamma d \to np\eta'$ cross section measured by CBELSA/TAPS.

$S_{11}(1920)$ seems to be needed in the reaction, with which the total cross section near threshold for $\gamma p \to \eta' p$ is improved slightly. However, the differential cross sections, excitation functions, and beam asymmetries are not sensitive to

$S_{11}(1920)$. To confirm $S_{11}(1920)$, more accurate observations are needed.

Furthermore, it should be mentioned that the polarized beam asymmetries are found to be sensitive to $D_{13}(1520)$, although its effects on the differential cross sections and total cross sections are negligible. There is no obvious evidence of the P-, D_{13}-, F-, and G-wave resonances with a mass around 2.0 GeV in the reactions.

To better understand the physics in the $\gamma p \to \eta' p$ and $\gamma n \to \eta' n$ reactions, we expect more accurate measurements of the following observables for both of the processes: (i) the total cross section in the energy region $E_\gamma \simeq 1.55 \sim 2.1$ GeV, (ii) the fixed-angle excitation functions at very forward angles from threshold up to $W \simeq 2.3$ GeV, (iii) the differential cross sections in the energy region $E_\gamma \simeq (1.6 \sim 1.9)$ GeV, and (iv) the beam asymmetries in the energy region $E_\gamma \simeq 1.6 \sim 2.0$ GeV.

ACKNOWLEDGMENTS

The authors thank B. Krusche for providing us the data of η' photoproduction off quasifree nucleons. This work is supported, in part, by the National Natural Science Foundation of China (Grants 10775145, 11075051, and 11035006), Chinese Academy of Sciences (KJCX2-EW-N01), Ministry of Science and Technology of China (2009CB825200), the Program for Changjiang Scholars and Innovative Research Team in University (PCSIRT, No. IRT0964), the Program Excellent Talent Hunan Normal University, and the Hunan Provincial Natural Science Foundation (11JJ7001).

[1] Aachen-Berlin-Bonn-Hamburg-Heidelberg-Munchen Collaboration, Phys. Rev. **175**, 1669 (1968).
[2] W. Struczinski *et al.* (Aachen-Hamburg-Heidelberg-Munich Collaboration), Nucl. Phys. B **108**, 45 (1976).
[3] R. Plotzke *et al.* (SAPHIR Collaboration), Phys. Lett. B **444**, 555 (1998).
[4] J. F. Zhang, N. C. Mukhopadhyay, and M. Benmerrouche, Phys. Rev. C **52**, 1134 (1995).
[5] Z. P. Li, J. Phys. G **23**, 1127 (1997).
[6] Q. Zhao, Phys. Rev. C **63**, 035205 (2001).
[7] B. Borasoy, Eur. Phys. J. A **9**, 95 (2000).
[8] A. Sibirtsev, C. Elster, S. Krewald, and J. Speth, AIP Conf. Proc. **717**, 837 (2004).
[9] W. T. Chiang, S. N. Yang, L. Tiator, M. Vanderhaeghen, and D. Drechsel, Phys. Rev. C **68**, 045202 (2003).
[10] K. Nakayama and H. Haberzettl, Phys. Rev. C **69**, 065212 (2004).
[11] M. Dugger *et al.*, Phys. Rev. Lett. **96**, 062001 (2006); **96**, 169905(E) (2006).
[12] M. Williams *et al.* (CLAS Collaboration), Phys. Rev. C **80**, 045213 (2009).
[13] V. Crede *et al.* (CBELSA/TAPS Collaboration), Phys. Rev. C **80**, 055202 (2009).
[14] I. Jaegle *et al.*, Eur. Phys. J. A **47**, 11 (2011).
[15] K. Nakayama and H. Haberzettl, Phys. Rev. C **73**, 045211 (2006).
[16] F. E. Close and Z. P. Li, Phys. Rev. D **42**, 2194 (1990).
[17] Q. Zhao, J. S. Al-Khalili, and C. Bennhold, Phys. Rev. C **64**, 052201 (2001).
[18] Z. P. Li, Phys. Rev. D **48**, 3070 (1993); **50**, 5639 (1994); Phys. Rev. C **52**, 1648 (1995).
[19] Z. P. Li, Phys. Rev. D **52**, 4961 (1995).
[20] Z. P. Li and B. Saghai, Nucl. Phys. A **644**, 345 (1998).
[21] B. Saghai and Z. P. Li, Eur. Phys. J. A **11**, 217 (2001).
[22] J. He, B. Saghai, and Z. P. Li, Phys. Rev. C **78**, 035204 (2008).
[23] J. He and B. Saghai, Phys. Rev. C **80**, 015207 (2009).
[24] Q. Zhao, B. Saghai, and Z. P. Li, J. Phys. G **28**, 1293 (2002).
[25] Q. Zhao, Z. P. Li, and C. Bennhold, Phys. Rev. C **58**, 2393 (1998); Phys. Lett. B **436**, 42 (1998).
[26] Z. P. Li, H. X. Ye, and M. H. Lu, Phys. Rev. C **56**, 1099 (1997).
[27] Q. Zhao, J. S. Al-Khalili, Z. P. Li, and R. L. Workman, Phys. Rev. C **65**, 065204 (2002).
[28] X. H. Zhong and Q. Zhao, Phys. Rev. C **84**, 045207 (2011).
[29] R. G. Moorhouse, Phys. Rev. Lett. **16**, 772 (1966).
[30] R. Dolen, D. Horn, and C. Schmid, Phys. Rev. **166**, 1768 (1968).
[31] R. A. Williams, C. R. Ji, and S. R. Cotanch, Phys. Rev. C **43**, 452 (1991).
[32] G. F. Chew, M. L. Goldberger, F. E. Low, and Y. Nambu, Phys. Rev. **106**, 1345 (1957).
[33] R. L. Walker, Phys. Rev. **182**, 1729 (1969).
[34] C. G. Fasano, F. Tabakin, and B. Saghai, Phys. Rev. C **46**, 2430 (1992).
[35] C. S. An and B. Saghai, Phys. Rev. C **84**, 045204 (2011).
[36] V. Crede *et al.* (CB-ELSA Collaboration), Phys. Rev. Lett. **94**, 012004 (2005).
[37] A. V. Anisovich, A. Sarantsev, O. Bartholomy, E. Klempt, V. A. Nikonov, and U. Thoma, Eur. Phys. J. A **25**, 427 (2005).
[38] A. V. Anisovich, E. Klempt, V. A. Nikonov, A. V. Sarantsev, and U. Thoma, arXiv:1109.0970.
[39] K. Nakamura *et al.* (Particle Data Group), J. Phys. G **37**, 075021 (2010).